Chaos, Solitons and Fractals 152 (2021) 111317

Contents lists available at ScienceDirect

Chaos, Solitons and Fractals

Nonlinear Science, and Nonequilibrium and Complex Phenomena

journal homepage: www.elsevier.com/locate/chaos

Frontiers

Oscillatory motion of dissipative solitons induced by delay-feedback in inhomogeneous Kerr resonators

F. Tabbert[a], S.V. Gurevich[a], K. Panajotov[b], M. Tlidi[c,*]

[a] Institute for Theoretical Physics, University of Münster, Wilhelm-Klemm-Str. 9, Münster D-48149, Germany
[b] Vrije Universiteit Brussel, Department of Applied Physics & Photonics, Pleinlaan 2, Brussels B-1050, Belgium
[c] Faculté des Sciences, Université Libre de Bruxelles (ULB), Campus Plaine, CP. 231, Bruxelles B-1050, Belgium

ARTICLE INFO

Article history:
Received 30 March 2021
Revised 8 July 2021
Accepted 24 July 2021
Available online 29 September 2021

2010 MSC:
00-01
99-00

Keywords:
Elsarticle.cls
LaTEX
Elsevier
Template

ABSTRACT

We investigate the destabilization mechanisms of dissipative solitons in inhomogeneous nonlinear resonators subjected to injection and to time-delayed feedback. We consider the paradigmatic Lugiato-Lefever model describing inhomogeneous driven nonlinear optical resonator. We analyze the pinning-depinning transition of dissipative solitons by introducing a potential induced by the inhomogeneity. Further, we identify conditions under which these structures are destabilized and describe different bifurcation scenarios. We show that the combined influence of inhomogeneities and delayed feedback induces an Andronov-Hopf-bifurcation that leads to oscillations of the dissipative soliton around the inhomogeneity. Finally, we show that for large values of the feedback strength, the dissipative solitons escapes from the potential well and starts to drift.

1. Introduction

Kerr resonators are optical devices capable of generating, in the frequency domain, combs with a spectrum that includes thousands of narrow lines precisely equidistant. These simple optical devices have been studied extensively for numerous applications, ranging from high-precision spectroscopy, metrology, and photonic analog-to-digital conversion (see a recent overview on this issue [1]). In particular, dissipative soliton (DS) frequency comb generation has attracted numerous research activities since their experimental evidence in micro-cavity resonators [2]. Dissipative soliton combs are the spectral content of the dissipative solitons or temporal cavity solitons. These combs are theoretically described in the mean-field limit by the well know Lugiato-Lefever equation (LLE, [3]). The link between frequency combs generated in optical Kerr resonators and stable dissipative solitons occurring in the cavity has been discussed in an excellent review by Lugiato and collaborators [4] in the theme issue [5]. The LLE constitutes a paradigm for the investigation of confinement of light in a driven high-Q cavity filled by a Kerr medium. Due to the richness of its spectrum of dynamical behaviors, the LLE has attracted considerable theoretical and experimental investigations these last decades. Dissipative Kerr soliton [6–8], front dynamics [9,10], spatio-temporal chaos [11], rogue waves are among the phenomena that have been predicted (see recent overview on the LLE, [12]).

When the Kerr resonators are driven by an inhomogeneous injected beam such as a modulated beam [13–15] or Gaussian [16], dissipative solitons can be stabilized through the front pinning mechanism. When the cavity is operating close to the modulational instability, it has been shown that the inhomogeneity impacts strongly the stability domains, as well as the homoclinic snaking bifurcation associated with the formation of dissipative solitons [17]. In particular, the stability domain of a single peak dissipative solitons is much larger than the pinning region where the system exhibits multistability between multiple peaks of dissipative solitons [17]. Dissipative soliton and localized pattern formation are an important issue not only in the context of nonlinear optics and laser physics but constitute a multidisciplinary area of research in many far from equilibrium extended systems involving physics, chemistry, biology, plant ecology, and mathematics (see overviews on this issue [18–24]).

Dissipative solitons are not always stationary, they can exhibit spontaneous motion induced by a regular delayed feedback [25–29], or a delayed Raman nonlocal response [30–32]. This regular motion occurs under a continuous wave injection. Other mechanisms leading to the motion of DSs such as the third-order dis-

* Corresponding author.
E-mail address: mtlidi@ulb.ac.be (M. Tlidi).

https://doi.org/10.1016/j.chaos.2021.111317
0960-0779/

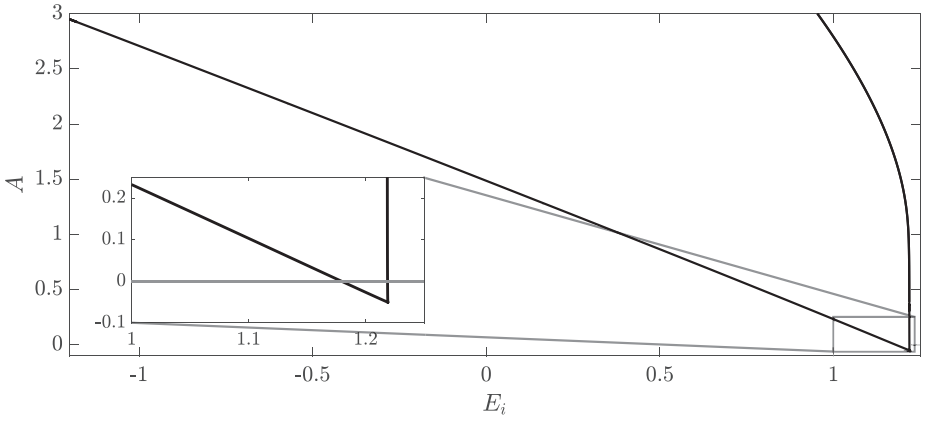

Fig. 1. Results of a fold continuation depicting the positions of the left and right folds delimiting the stability of a single DS as a function of A and E_i. In between the two lines, single DS exists and is stable. The widening effect when increasing the amplitude of the inhomogeneity is again visible. The inset emphasizes, that a single DS pinned on the center also exists for a negative A, although it is unstable (compare with Fig. 3). At a value of $A \approx -0.05$, the two folds collide, i.e., for lower values of A, no DS pinned on the center of the inhomogeneity exists.

persion effect have been reported [33–37]. Nonlinear gradient convection term in the cubic complex Ginzburg-Landau can lead to the drift of dissipative solitons [38,39]. The influence of inhomogeneities and convection [40,41], or delayed feedback have been also investigated for the Swift-Hohenberg equation [42]. The combined influence of the delay feedback and the third order dispersion has also been studied [43].

In this paper, we investigate the combined influence of inhomogeneities in a Kerr resonator and the time-delayed feedback on the stability of dissipative solitons. We consider an inhomogeneous Kerr resonator with a delayed feedback loop. This simple device is described by the delayed LLE. We show that for a moderate feedback strength, inhomogeneity in the injected field can arrest the drift of the dissipative solitons, and allow for regular time oscillations around the defect. We attribute this regular oscillation to the balance between two opposite effects: an attractive, pinning effect by the inhomogeneity and the drift induced by the time-delayed feedback. From a dynamical point of view, we show that for a moderate feedback strength, a single DS undergoes an Andronov-Hopf bifurcation leading to oscillations around the inhomogeneity. However, for larger feedback strengths, the dissipative soliton can escape from the potential well and start to drift.

The paper is organized as follows, after a brief introduction, we discuss in Section 2, the formation of dissipative solitons in the presence of inhomogeneities. This effect has been discussed in [17] for a small and positive defect, here we investigate more systematically the effect of inhomogeneities including the case when the amplitude of the defect is negative. We analyze this effect by using the tools of bifurcation theory, showing that depending on the system parameters, the inhomogeneity can attract or repeal dissipative solitons. The associated homoclinic snaking bifurcation diagram is constructed using continuation algorithms provided by the Matlab continuation package pde2path [44]. In Section 3, we investigate the combined action of inhomogeneities and the time-delayed feedback on the stability of dissipative solitons in the LLE. We conclude in Section 4.

2. The inhomogeneous Lugiato–Lefever model

We consider a Kerr resonator subjected to an inhomogeneous injected field and delayed feedback. In the mean-field limit, the dimensionless Lugiato-Lefever equation reads [3]

$$\frac{\partial E(t,\xi)}{\partial t} = S(\xi) + \left[-(1+i\theta) + i|E(t,\xi)|^2 + i\frac{\partial^2}{\partial \xi^2}\right]E(t,\xi). \quad (1)$$

Here, the intracavity field envelope is denoted by $E(t,\xi)$, θ is the detuning parameter and $S(\xi)$ is the inhomogeneous injected field

$$S(\xi) = E_i + A\ \exp(-\xi^2/B),$$

where E_i is the homogeneous value of the injection, A and B correspond to the amplitude and the width of the Gaussian shape in homogeneity, respectively. Depending on the context in which the LLE is derived, ξ is the transverse coordinate or the fast time in the reference frame moving with the group velocity of the light within the cavity while t is the slow time proportional to the round-trip time. The LLE (1) model is valid under the assumptions of high resonator finesse, small nonlinearity, and a dispersion length much larger than the cavity length. The LLE Eq. (1) has broad applicability than passive optical cavities (see recent a overview [45]).

We examine the case of a monostable system where the modulational instability appears subcritical, i.e., $\theta > 41/30$, where the homogeneous steady state coexists with a periodic structure that emerges from the modulational instability. In addition, the system exhibits a high degree of multistability in a finite range of S values often called the pinning region [6,7]. Eq. (1) supports an infinite set of odd and even number of peaks forming a stationary DSs. The influence of inhomogeneities on the stability of dissipative solitons has been studied for small positive inhomogeneities $A > 0$. Two or more peak DS are bounded together by their decaying oscillatory tails, and therefore, their bifurcation diagram has homoclinic snaking structure [8]. The stability, bifurcation properties, and the position of DSs are strongly affected by the inhomogeneity. A small positive inhomogeneity $A > 0$ acts attracting on the DS [17]. In what follows we investigate the effect of the inhomogeneity more systematically by exploring positive and negative values of the parameter A that controls the amplitude of the defect. A visualization of this fold continuation is shown in Fig. 1, where the positions of the left and right folds are depicted in an $A - E_i$ diagram. As can be seen, the widening of the region of stability is rather consistent for small to moderate values of the inhomogeneity, as a notable shift of the right fold sets in only at $A \approx 1.0$. The inset illustrates that, although positive values of A act attracting on DS in this parameter regime, the DS pinned on the center of the inhomogeneity also persist for small negative values of the inhomogeneity before both folds collide at $A \approx -0.05$ and the DS vanishes for values of $A < -0.05$. However, as will be shown in the following, the DS on the center of the inhomogeneity only exists as unstable solution in this rather narrow regime of negative A.

This observation brings up the question, which kind of DS, if any, exists for negative values of A. We therefore perform a sim-

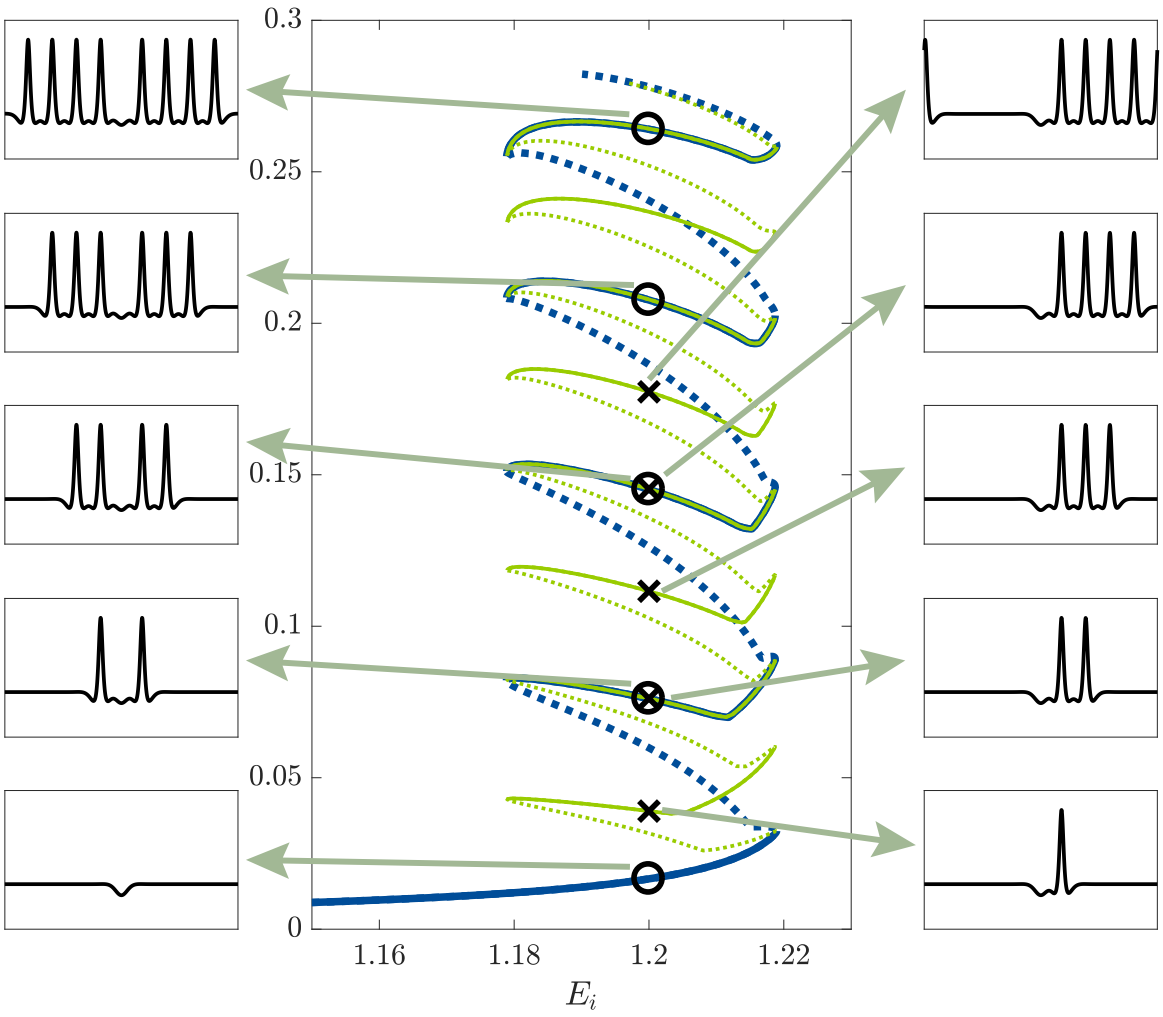

Fig. 2. Bifurcation diagram of DSs. The norm L_1 as a function of the injected field amplitude E_i undergoes a homoclinic snaking type of bifurcation in the presence of an inhomogeneity with a negative amplitude of $A = -0.1$. Other parameters are $\theta = 1.7$ and $B = 0.4$. The quasi-homogeneous solution (lowest branch, solution profile depicted on the lower left) evolves into a solution with a peak on each side of the inhomogeneity. This branch (blue line) undergoes the classical homoclinic snaking, with additional peaks growing on each side throughout the snaking. Solution profiles at the positions marked by circles are depicted on the left. Shortly before the first fold of the even branch, a single peak solution (solution profile on the lower right) bifurcates in a subcritical pitchfork bifurcation. This solution undergoes a symmetry broken snaking where with each turn only one peak is added to the solution profile. Peaks are only added on the far side of the inhomogeneity. Solution profiles at the positions marked by the crosses are depicted on the right. Both the green and the blue branch overlap substantially, since e.g., a two-peak solution possesses essentially the same L_1-norm, regardless of the position of the peaks. It should be noted, that none of the branches connects to a periodic or a quasi-periodic solution. If one continues to follow the branch they wind down again towards lower peak solutions. (For interpretation of the references to colour in this figure legend, the reader is referred to the web version of this article.)

ilar analysis by means of numerical continuation, starting now with the quasi-homogeneous solution for a small negative value of $A = -0.1$. Since the amplitudes of DSs having different numbers of peaks are close to one another, it is convenient to plot the dimensionless "L_1 norm,"

$$L_1 = \int d\xi \, |E - E_m|^2 \tag{2}$$

as a function of the injected field amplitude, where E_m denotes the mean value of the electrical field $E(\xi)$ averaged over the domain size. The results are summarized in Fig. 2, showing the bifurcation diagram in the center of the figure and the quasi-homogeneous solution on the bottom left. When the "L_1 norm" is increased, at each turning point (fold) where the slope becomes infinite, a pair of additional peaks appears in the cluster showing a close resemblance to the case without inhomogeneities. In contrast to the case of homogeneous injection, the snaking diagram does not connect to a homogeneous solution but starts to wind down again, once the domain is filled with peaks. With increasing A, the quasi-homogeneous solution (lowest blue branch) becomes destabilized in a subcritical pitchfork bifurcation immediately followed by a fold. Following the blue branch, a pair of peaks forms at either side of the inhomogeneity.

It is also worthwhile to take a closer look at the subcritical pitchfork bifurcation close to the first fold in which an odd solution (green) branch bifurcates from the quasi-homogeneous solution. On this branch a single peak solution with one peak pinned on the side of the inhomogeneity is formed. This uneven branch resembles in its origin and in its solution profile the so-called ladders [46]. Following the green branch, solution profiles at the positions marked with a cross are depicted on the right-hand side of Fig. 2, showing that in this symmetry-broken version of a homoclinic-snaking diagram, peaks are not added in pairs to the solution but the solution gains additional peaks one by one. Since the depicted L_1-norm of an n-peak solution does not differ greatly for different peak positions, the green and the blue branch overlap when both branches show an even number of peaks. One can note that similar bifurcations to the one leading to the emergence of the green branch can be found close to every fold of the blue branch as is the case with the so-called ladders [46]. The additional branches

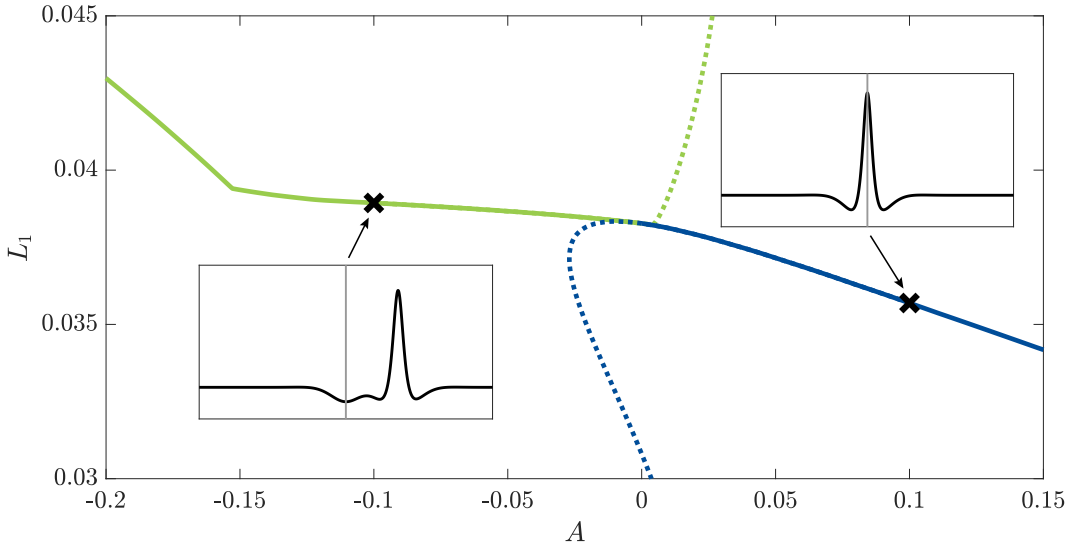

Fig. 3. Continuation with A as the continuation parameter for $\theta = 1.7$, $E_i = 1.2$. As suggested by the previous results, the solution pinned on the center (blue line, right inset) is stable for positive A, while the solutions pinned on either side of the inhomogeneity (left inset, green line) are stable for negative A. The two solution types interchange stability in a transcritical bifurcation at $A = 0$. The centered solution exists (although unstable) in a narrow parameter regime of negative A before turning in a fold. The same scenario is valid for the solution pinned on the side for positive A. (For interpretation of the references to colour in this figure legend, the reader is referred to the web version of this article.)

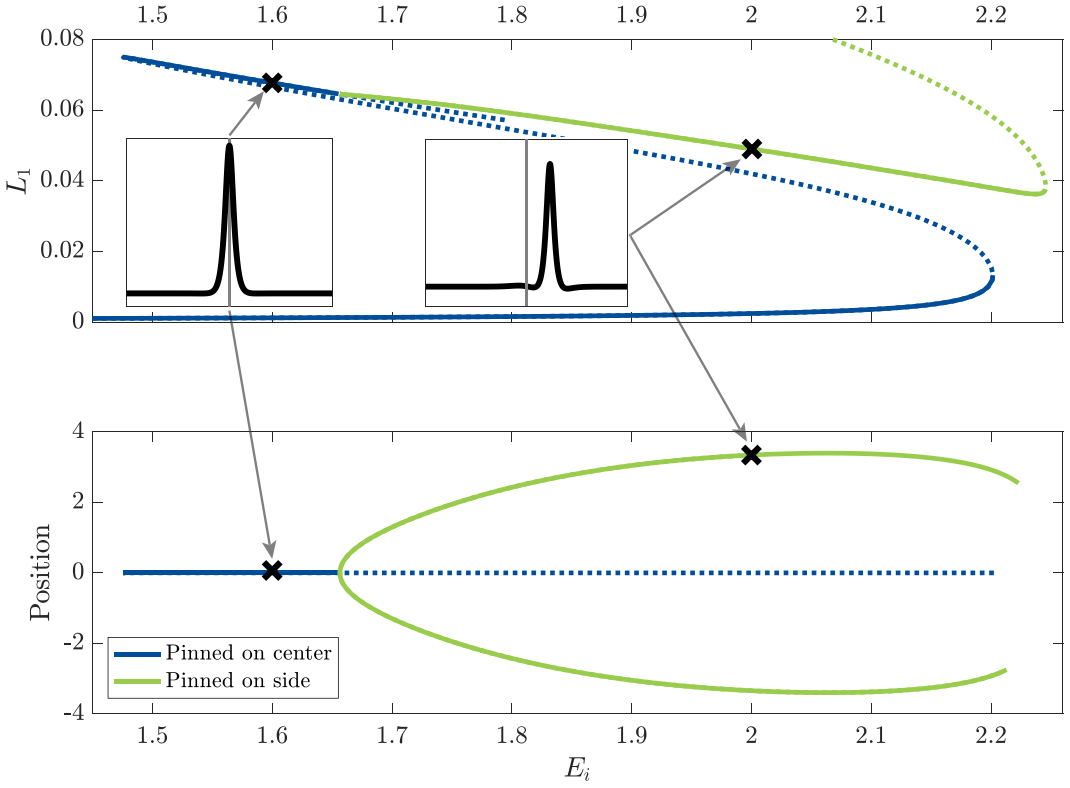

Fig. 4. Emergence of a single DS in the non-snaking regime of $\theta = 3.0$ for an inhomogeneity with $A = 0.1$, $B = 4.0$. The continuation parameter is E_i. On the vertical axis, we use the L_1-norm (top) and the position (bottom) respectively. The stable DS pinned on the center arises from the quasi-homogeneous solution in a sequence of two folds (blue line). Unlike the case of lower θ, the solution pinned on the center (blue line, left inset) looses stability in a supercritical pitchfork bifurcation at $E_i \approx 1.66$ with respect to translational perturbations. Two new DS solutions positioned on either side of the inhomogeneity (green line, right inset) arise. The characteristic pitchfork shape of the bifurcation diagram is better visible in the lower representation, since the left and the right solution coincide when solely depicting the L_1-norm. (For interpretation of the references to colour in this figure legend, the reader is referred to the web version of this article.)

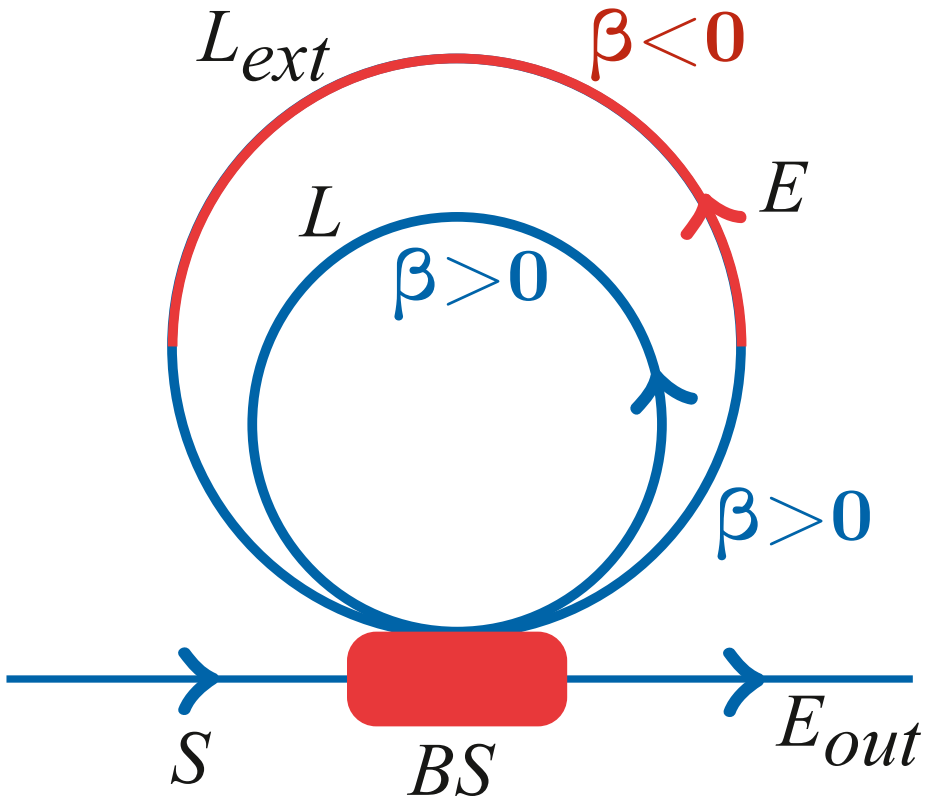

Fig. 5. Schematic representation of a ring nonlinear cavity with external feedback delayed loop. BS denotes the beam splitter. We assume that the dispersion in the external cavity of length L_{ext} is compensated by periodic group velocity dispersion management with zero average value, i.e., half with $\beta > 0$ and the other half with $\beta > 0$ where β is the second-order chromatic dispersion coefficient.

emerging from these bifurcations are not depicted in Fig. 2 for the sake of clarity but these branches would also exhibit solutions that show an uneven number of peaks on each side of the inhomogeneity. Therefore, not only the completely symmetric and the completely asymmetric case as depicted in Fig. 2 are possible, but every configuration of peaks on either side of the inhomogeneity. Fig. 3 shows the results of numerical continuation for fixed θ and fixed injection. The green line depicts the solutions pinned on the side, which are stable for $A < 0$, while the blue line depicts the solutions pinned at the center of inhomogeneities, which are stable for $A > 0$. Both solutions interchange their stability in a transcritical bifurcation at $A=0$. When the detuning parameter is high small and starting with small inhomogeneity of $A = 0.1$, we first deploy a parameter continuation in E_i starting from the quasi-homogeneous solution. Fig. 4 on the top shows, that the emergence of single DSs from the quasi-homogeneous solution (blue line). In two consecutive folds, the solution goes from the quasi-homogeneous solution to a DS pinned on the center of the inhomogeneity (blue line). In contrast to the case of lower detuning, another bifurcation sets in at $E_i \approx 1.66$. In a supercritical pitchfork bifurcation, the DS pinned on the center of the inhomogeneity (blue line) loses stability and two stable solutions emerge (green line), which move away from the center with increasing E_i until they come to a halt at the side of the inhomogeneity. The depiction on the bottom half of Fig. 4 emphasizes this pitchfork bifurcation by using the center of mass position as a measure instead of the L_1-norm.

3. Interplay between spatial inhomogeneities and time-delay

We consider a Kerr resonator subjected to an inhomogeneous injected field and to delayed feedback governed by the Lugiato-Lefever equation. We implement the time delayed feedback control scheme as the difference between the system variables at the current moment of time and their values at a fixed time in the past which is also referred to as Pyragas control [47]. This cavity can be a fiber resonator [9,10] or whispering-gallery disk microresonators [48] with of radius $L/2\pi$. The schematic representation of the setup of a ring nonlinear cavity with an external feedback delayed loop is shown in Fig. 5. We assume that the ring cavity operates in an anomalous dispersion regime ($\beta > 0$). The delayed feedback is introduced by an external loop with a large radius $L_{ext}/2\pi$, as shown schematically in Fig. 5. The delay time $\tau = L_{ext}n/c$ corresponds to the light travel-time in the external loop with c and n are respectively the speed of light and the effective refractive index of the fiber. The LLE with delayed feedback reads [27,28]

$$\frac{\partial E}{\partial t} = S(\xi) + \left[-(1+i\theta) + i|E|^2 + i\frac{\partial^2}{\partial \xi^2}\right]E + \eta e^{i\phi}[E(t,\xi) - E(t-\tau,\xi)]. \tag{3}$$

The delayed feedback is characterized by the feedback strength η, the phase ϕ, and the delay time τ. To analyze instabilities of stationary solutions of Eq. (3), we perform a linear stability analysis in the presence of delayed feedback. In the case of a Pyragas control scheme, the eigenmodes of the system keep their spatial form. For a fixed feedback phase ($\phi = \pi$ or $\phi = 0$), the eigenvalues λ can be calculated by evaluating [26]

$$\lambda_m = \mu + \eta + \frac{1}{\tau}W_m\left[-\eta\tau e^{-\tau(\mu+\eta)}\right], \tag{4}$$

where $m \in \mathbf{Z}$ and W_m is the m th branch of the Lambert W function [49] and μ is the eigenvalue in the absence of delayed feedback. Note that for every eigenvalue μ of the undelayed system, there

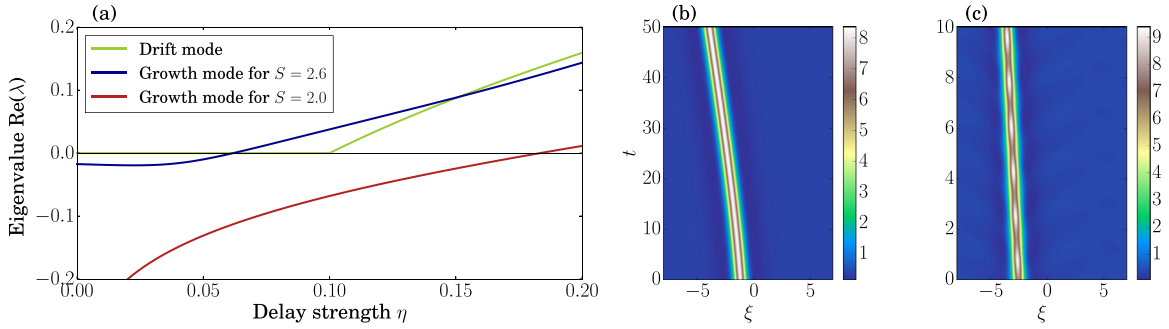

Fig. 6. Dynamics of DS in a homogeneous Kerr cavity. (a): Real parts of the eigenvalues Re(λ) as a function of η. The green line corresponds to the eigenvalue of the neutral mode leading to the drift bifurcation at $\eta\tau = 1$. The bifurcation point of the growth mode inducing the AH bifurcation depends on the parameters S and θ. The blue and red curves indicate a case when the AH bifurcation occurs before ($S = 2.6$) and after ($S = 2.0$) the drift bifurcation, respectively. (b),(c): Space-time maps showing the evolution of the intracavity intensity obtained by numerical integration of Eq. (3). (b) Drifting DS obtained for $S = 2.0$ and $\eta = 0.13$; (c) Self-pulsating and drifting DS obtained for $S = 2.0$ and $\eta = 0.19$. Other parameters are $\tau = 10$ and $\theta = 3.5$. (For interpretation of the references to colour in this figure legend, the reader is referred to the web version of this article.)

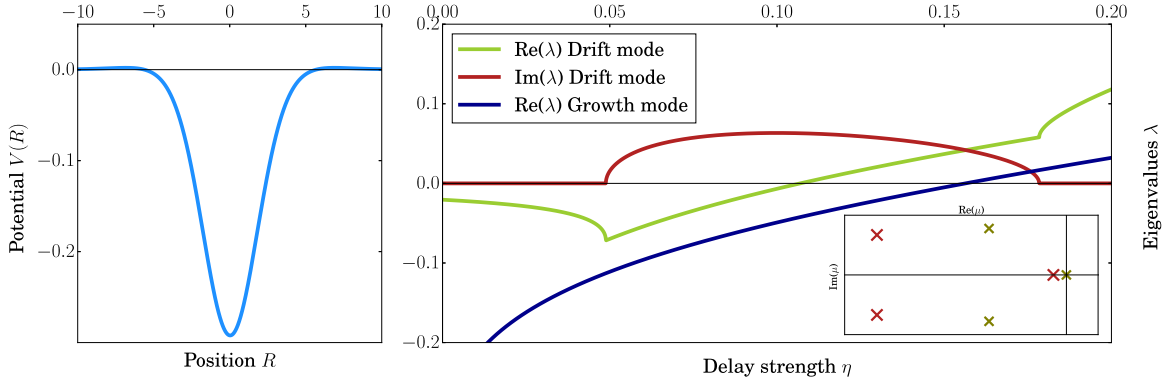

Fig. 7. Left: Potential induced by an inhomogeneity in the injection field with $A = -0.3$, $B = 4.0$ in the LLE Eq. (3) with $E_i = 2.3$, $\theta = 3.5$. The potential acts attracting and pulls the DS towards its center. However, at the border of the potential well, the potential shows narrow regions where it acts repelling on the DS. Right: Real (green) and imaginary (red) part of the eigenvalue of the drift inducing mode as well as the real part of the eigenvalue of the growth inducing mode for different values of η and fixed $\tau = 10.0$. In contrast to the homogeneous case $A = 0$ described in Fig. 6, the eigenvalue λ of the drift inducing mode becomes complex around the onset of instability, suggesting an oscillatory behavior. The growth inducing mode becomes unstable in a second AH bifurcation at larger values of η. Inset: First three eigenvalues μ without delay, with (red) and without (green) inhomogeneity. The pinning effect of the inhomogeneity is clearly visible, lowering the eigenvalues of both the drift inducing mode and the growth inducing mode. (For interpretation of the references to colour in this figure legend, the reader is referred to the web version of this article.)

exists an infinite number of corresponding eigenvalues λ_m with delay. However, when considering destabilization scenarios for a given eigenvalue μ, one usually only has to take into account the eigenvalue λ_0 generated by the main branch W_0 of the Lambert W function. In any spatially homogeneous system ($A = 0$), the neutral mode corresponding to $\mu = 0$, induces a pitchfork bifurcation at $\eta\tau = 1$ leading to a drift of the DS [25,26]. In the case of the LLE Eq. (3) two additional critical complex eigenvalues exist (cf. Fig. 7, inset), corresponding to an even mode that leads to a change of the size of the DS when it is destabilized by the delayed feedback. We therefore refer to this mode as growth mode. Depending on the parameter values of E_i and θ, this Andronov-Hopf instability (AH) may occur either before or after the drift instability when increasing the feedback strength η for a fixed value of τ (see Fig. 6 (a)). An example of a drifting DS in a homogeneous system is shown in (Fig. 6 (b)) for the case where only the drift mode is destabilized. A self-pulsating and drifting DS is shown in (Fig. 6) where both the drift and the growth mode are destabilized. In the next section, we investigate the effect of an inhomogeneous injected beam on the dynamics of the DS induced by delayed feedback.

By introducing a spatial inhomogeneity to the injection S, the translational symmetry of the system is broken. The effect of the inhomogeneity in the injection field depends on the sign of the parameter A. If $A < 0$ ($A > 0$), the inhomogeneity attracts (repells) the DS. In the following we focus on attractive inhomogeneities, i.e., $A < 0$. By using the approach described in [17], one can estimate the attracting potential induced by the inhomogeneity acting on a single DS. This potential is plotted as a function of the relative position R between the maximum of the DS and the minimum of the inhomogeneity of the injected beam in Fig. 7 (left). In the bistable regime $\theta > \sqrt{3}$ we are interested in, the oscillating tails of the DS in the LL-model Eq. (3) are less pronounced than in the Swift-Hohenberg model discussed in [42], therefore, there are only very narrow regions on the side of the potential, where the DS gets repelled. A DS positioned between those regions gets pulled to the center of the inhomogeneity, corresponding to the minimum of the potential. As the DS gets pinned by the inhomogeneity, both the eigenvalue of the drift mode and the real parts of the eigenvalues corresponding to the growth mode are lowered (Fig 7, inset). Note that the pinning of the DS is obtained in the case when the delayed feedback control is absent and is only a result of the attracting inhomogeneity. In the following we are discussing the destabilization of a such pinned DS by time-delayed feedback.

Since the eigenvalue of the drift mode in the absence of time-delayed feedback is $\mu \neq 0$, evaluating Eq. (4) leads to complex eigenvalues $\lambda \in \mathbf{C}$. For fixed τ, the real and the imaginary parts of the eigenvalue λ of the drift mode are shown in Fig. 7 (right) as a function of the delay strength η. At the bifurcation point, i.e., $\mathrm{Re}(\lambda) = 0$, the imaginary part is non-vanishing. This means that in this case an AH bifurcation takes place allowing oscillatory behavior. Note, however, that without delayed feedback, the inhomo-

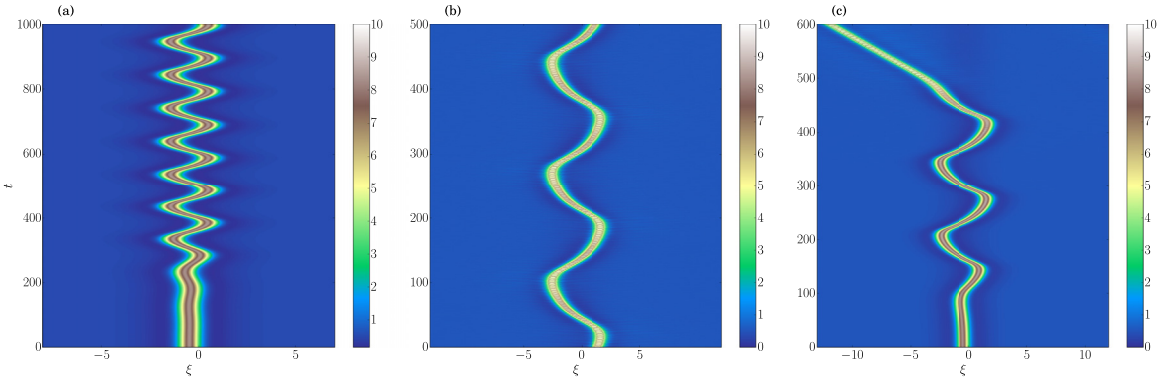

Fig. 8. (a-c): Space-time maps in (ξ, t) plane showing the intensity field obtained by direct numerical simulations of Eq. (3) with an inhomogeneity in the injected field for $E_i = 2.3$, $\theta = 3.5$, $A = -0.3$, $\tau = 10.0$ and increasing values of η. (a) $\eta = 0.13$: The destabilization of the drift inducing mode in a Andronov-Hopf bifurcation leads to an oscillatory motion of the DS. (b) $\eta = 0.15$: The unstable growth modes leads to an additional oscillation in size of the LS. (c) $\eta = 0.16$: The increased feedback strength leads to the depinning of the DS from the inhomogeneity.

geneity has an even stronger stabilizing effect on the eigenvalues corresponding to the growth mode than on the eigenvalue of the drift mode (cf. Fig. 7, inset). Therefore, the destabilization of the growth mode occurs after the drift bifurcation when increasing the strength of the delayed feedback in the inhomogeneous case (see Fig. 7, right).

By evaluating Eq. (4) in the inhomogeneous case, one can identify different regions of stability and perform direct numerical simulations to analyze how the instability of the two different modes affects the dynamical behavior of the DS. Due to the pinning effect of the inhomogeneity, the drift threshold is not at $\eta\tau = 1$ anymore but at larger values of the delay parameters. For a fixed value of the delay time $\tau = 10.0$, the threshold is $\eta \approx 0.107$. Numerical simulations performed above this threshold at $\eta = 0.13$ show that the unstable drift mode with a complex eigenvalue leads to a drift of the DS, yet the attracting force of the potential pulls the structure back to its center. The competition between destabilizing delay and an attracting inhomogeneity leads to an oscillation with constant amplitude. For larger delay strengths $\eta = 0.16$, the effects of the growth mode become visible by a slight oscillation in the shape of the structure as shown in Fig. 8(b). This behavior can be explained by the fact that the system just underwent the second AH bifurcation at $\eta \approx 0.1564$. Finally, for larger values of $\eta = 0.165$, the force induced by the delayed feedback becomes strong enough to push the DS out of the potential well induced by the inhomogeneity and the structure starts to drift freely. This depinning process is depicted in Fig. 8(c).

4. Conclusions

We have considered the Lugiato-Lefever equation describing light propagation in a driven Kerr resonator. In the first part, we have investigated the stability properties of dissipative soliton under an inhomogeneous injection in the form of Gaussian beam. In the case where A is positive, the inhomogeneity acts attracting on dissipative solitons [17]. This means that DS is pinned on the center of the inhomogeneity. However, for negative A, the inhomogeneity acts repelling on dissipative soliton. In this case, the dissipative soliton is pinned on the side of the inhomogeneity rather than on its center. We have constructed the homoclinic snaking diagram associated with the formation of Kerr dissipative solitons.

In the second part, we discuss the destabilization mechanisms of a single dissipative soliton under the combined influence of time-delayed feedback and inhomogeneous injection. We first report on two different bifurcations in the case of a continuous wave operation in the presence of delayed feedback. We then investigate the influence of an inhomogeneous injection field. In both cases two modes can be destabilized, the drift-inducing mode and a size changing mode we referred to as growth mode. Whereas the growth mode always becomes unstable in an Andronov-Hopf bifurcation leading to oscillations of the dissipative solitons width, the drift mode becomes unstable in two different bifurcation scenarios: In the homogeneous case, the DS undergoes a pitchfork bifurcation leading to a drift of the DS. However, in the inhomogeneous case discussed, the drift mode becomes unstable in an Andronov-Hopf bifurcation leading to oscillations of the dissipative soliton around the inhomogeneity. This behavior occurs for moderate values of the delay strength. When increasing the strength of the delay for a fixed delay time, the dissipative solitons escapes from the potential well and starts to drift freely.

We have shown that even in the presence of small inhomogeneities, the delay-induced dynamics change drastically due to the pinning effect of the inhomogeneity. Inhomogeneities are inherent in any nonlinear optical cavity. They occur either naturally due to impurities or are introduced intentionally by accordingly designed experimental setups. Our results can then be applied to various spatially extended systems subjected to delayed feedback and inhomogeneities. Therefore it is necessary and promising to take into account the effects of inhomogeneities when analyzing dynamics of dissipative solitons in these systems.

Funding

F.T. received support from the German scholarship foundation and the Center for Nonlinear Science (CeNoS), Münster. K.P. acknowledges the support by the Fonds Wetenschappelijk Onderzoek-Vlaanderen FWO (G0E5819N) and the Methusalem Foundation. M.T acknowledges financial support from the Fonds de la Recherche Scientifique FNRS under Grant CDR no. 35,333,527 “Semiconductor optical comb generator”. A part of this work was supported by the “Laboratoire Associé International” University of Lille - ULB on “Self-organisation of light and extreme events” (LAI-ALLURE).”

Declaration of Competing Interest

The authors declare that they have no known competing financial interests or personal relationships that could have appeared to influence the work reported in this paper.

References

[1] Fortier T, Baumann E. 20 Years of developments in optical frequency comb technology and applications. Communications Physics 2019;2:1.

[2] Herr T, Brasch V, Jost JD, Wang CY, Kondratiev N, Gorodetsky ML, et al. Temporal solitons in optical microresonators. Nat Photonics 2014;8:145.
[3] Lugiato LA, Lefever R. Spatial dissipative structures in passive optical systems. Phys Rev Lett 1987;58:2209.
[4] Lugiato LA, Prati F, Gorodetsky ML, Kippenberg TJ. From the lugiato-lefever equation to microresonator-based soliton kerr frequency combs. Phil Trans R Soc A 2018;376:20180113.
[5] Tlidi M, Clerc MG, Panajotov K. Dissipative structures in matter out of equilibrium: from chemistry, photonics and biology, the legacy of ilya prigogine (part 1). Phil Trans R Soc A 2018;376:20180114.
[6] Scroggie AJ, Firth WJ, McDonald GS, Tlidi M, Lefever R, Lugiato LA. Pattern formation in a passive kerr cavity. Chaos Solitons Fractals 1994;4:1323.
[7] Tlidi M, Mandel P, Lefever R. Localized structures and localized patterns in optical bistability. Phys Rev Lett 1994;73:640.
[8] Gomila D, Scroggie AJ, Firth WJ. Bifurcation structure of dissipative solitons. Physica D 2007;227:70.
[9] Coen S, Tlidi M, Emplit P, Haelterman M. Convection versus dispersion in optical bistability. Phys Rev Lett 1999;83:2328.
[10] Garbin B, Wang Y, Murdoch SG, Oppo G-L, Coen S, Erkintalo M. Experimental and numerical investigations of switching wave dynamics in a normally dispersive fibre ring resonator. Eur Phys J D 2017;71:240.
[11] Liu Z, Ouali M, Coulibaly S, Clerc MG, Taki M, Tlidi M. Characterization of spatiotemporal chaos in a kerr optical frequency comb and in all fiber cavities. Opt Lett 2017;42:1063.
[12] Chembo YK, Gomila D, Tlidi M, Menyuk CR. Theory and applications of the lugiato-lefever equation. Eur Phys J D 2017;71:299.
[13] Staliunas K. Midband dissipative spatial solitons. Phys Rev Lett 2003;91:053901.
[14] Vladimirov A, Skryabin DV, Kozyreff G, Mandel P, Tlidi M. Bragg localized structures in a passive cavity with transverse modulation of the refractive index and the pump. Opt Express 2006;14:1.
[15] Kumar S, Herrero R, Botey M, Staliunas K. Taming of modulation instability by spatio-temporal modulation of the potential. Sci Rep 2015;5:1.
[16] Odent V, Tlidi M, Clerc MG, Glorieux P, Louvergneaux E. Experimental observation of front propagation in a negatively diffractive inhomogeneous kerr cavity. Phys Rev A 2014;90:011806(R).
[17] Tabbert F, Frohoff-Hülsmann T, Panajotov K, Tlidi M, Gurevich SV. Stabilization of localized structures by inhomogeneous injection in kerr resonators. Phys Rev A 2019;100:013818.
[18] Arecchi FT, Boccaletti S, Ramazza P. Pattern formation and competition in nonlinear optics. Phys Rep 1999;318:1.
[19] Akhmediev N, Ankiewicz A, editors. Dissipative solitons: from optics to biology and medicine. Springer Science & Business Media; 2008.
[20] Ackemann T, Firth W, Oppo GL. Fundamentals and applications of spatial dissipative solitons in photonic devices. Advances in atomic, molecular, and optical physics 2009;57:323.
[21] Purwins H-G, Bodeker H, Amiranashvili S. Dissipative solitons. Adv Phys 2010;59:485.
[22] Tlidi M, Staliunas K, Panajotov K, Vladimiorv AG, Clerc MG. Localized structures in dissipative media: from optics to plant ecology. Phil Trans R Soc A 2014;372:20140101.
[23] Tlidi M, Clerc MG. Nonlinear dynamics: materials, theory and experiments. In: Springer Proceedings in Physics, vol. 173; 2016.
[24] Clerc MG, Coullet P, Rojas R, Tlidi M. Introduction to focus issue: instabilities and nonequilibrium structures. Chaos 2020;30:110401.
[25] Tlidi M, Vladimirov AG, Pieroux D, Turaev D. Spontaneous motion of cavity solitons induced by a delayed feedback. Phys Rev Lett 2009;103:103904.
[26] Gurevich SV, Friedrich R. Instabilities of localized structures in dissipative systems with delayed feedback. Phys Rev Lett 2013;110:014101.
[27] Panajotov K, Puzyrev D, Vladimirov AG, Gurevich SV, Tlidi M. Impact of time-delayed feedback on spatiotemporal dynamics in the lugiato-lefever model. Phys Rev A 2016;93:043835.
[28] Tlidi M, Panajotov K, Ferré M, Clerc MG. Drifting cavity solitons and dissipative rogue waves induced by time-delayed feedback in kerr optical frequency comb and in all fiber cavities. Chaos 2017;27:114312.
[29] Tchakounte FM, Nana VB, Nana L. Time-delayed feedback with global and local contributions on spatiotemporal dynamics of waves in fiber cavity. Eur Phys J Plus 2021;136:1.
[30] Clerc MG, Coulibaly S, Tlidi M. Time-delayed nonlocal response inducing traveling temporal localized structures. Phys Rev Research 2020;2:013024.
[31] Clerc MG, Coulibaly S, Parra-Rivas P, Tlidi M. Nonlocal raman response in kerr resonators: moving temporal localized structures and bifurcation structure. Chaos 2020;30:083111.
[32] Parra-Rivas P, Coulibaly S, Clerc MG, Tlidi M. Influence of stimulated raman scattering on kerr domain walls and localized structures. Phys Rev A 2021;103:013507.
[33] Tlidi M, Bahloul L, Cherbi L, Hariz A, Coulibaly S. Drift of dark cavity solitons in a photonic-crystal fiber resonator. Phys Rev A 2013;88:035802.
[34] Parra-Rivas P, Gomila D, Gelens L. Coexistence of stable dark-and bright-soliton kerr combs in normal-dispersion resonators. Phys Rev A 2017;95:053863.
[35] Vladimirov AG, Gurevich SV, Tlidi M. Effect of cherenkov radiation on localized-state interaction. Phys Rev A 2018;97:013816.
[36] Hariz A, Bahloul L, Cherbi L, Panajotov K, Clerc M, Ferré MA, Kostet B, Averlant E, Tlidi M. Swift-hohenberg equation with third-order dispersion for optical fiber resonators. Phys Rev A 2019;100:023816.
[37] Vladimirov AG, Tlidi M, Taki M. Dissipative soliton interaction in kerr resonators with high-order dispersion. Phys Rev A 2021;103:063505.
[38] Descalzi O, Cisternas J, Brand HR. Mechanism of dissipative soliton stabilization by nonlinear gradient terms. Phys Rev E 2019;100:052218.
[39] Descalzi O, Brand HR. Dissipative soliton stabilization by several nonlinear gradient terms. Chaos 2020;30:043119.
[40] Parra-Rivas P, Gomila D, Matías MA, Colet P. Dissipative soliton excitability induced by spatial inhomogeneities and drift. Phys Rev Lett 2013;110:064103.
[41] Parra-Rivas P, Gomila D, Matías MA, Colet P, Gelens L. Competition between drift and spatial defects leads to oscillatory and excitable dynamics of dissipative solitons. Phys Rev E 2016;93:012211.
[42] Tabbert F, Schelte C, Tlidi M, Gurevich SV. Delay-induced depinning of localized structures in a spatially inhomogeneous swift-hohenberg model. Phys Rev E 2017;95:032213.
[43] Schelte C, Camelin P, Marconi M, Garnache A, Huyet G, Beaudoin G, Sagnes I, Giudici M, Javaloyes J, Gurevich SV. Third order dispersion in time-delayed systems. Phys Rev Lett 2019;123:043902.
[44] Uecker H, Wetzel D, Rademacher JDM. Pde2path-a matlab package for continuation and bifurcation in 2d elliptic systems. Numer Math Theory Methods Appl 2014;7:58.
[45] Ferré MA, Clerc MG, Coulibally S, Rojas RG, Tlidi M. Localized structures and spatiotemporal chaos: comparison between the driven damped sine-gordon and the lugiato-lefever model. Eur Phys J D 2017;71:1.
[46] Burke J, Knobloch E. Localized states in the generalized swift-hohenberg equation. Phys Rev E 2006;73:056211.
[47] Pyragas K. Continuous control of chaos by self-controlling feedback. Phys Lett A 1992;170:421.
[48] Chembo YK, Menyuk CR. Spatiotemporal lugiato-lefever formalism for kerr-comb generation in whispering-gallery-mode resonators. Phys Rev A 2013;87:053852.
[49] Corless RM, Gonnet GH, Hare DEG, Jeffrey DJ, Knuth DE. On the lambert w function. Adv Comput Math 1996;5:329.